Biophysics and Structure of the Patch and the Gigaseal

Thomas M. Suchyna,[†*] Vladislav S. Markin,[‡] and Frederick Sachs[†]
[†]State University of New York at Buffalo, Department of Physiology and Biophysics, Buffalo, New York 14214; and [‡]Departments of Anesthesiology and Pain Management and Biomedical Engineering, University of Texas Southwestern Medical Center, Dallas, Texas 75235-9068

ABSTRACT Interpreting channel behavior in patches requires an understanding of patch structure and dynamics, especially in studies of mechanosensitive channels. High resolution optical studies show that patch formation occurs via blebbing that disrupts normal membrane structure and redistributes in situ components including ion channels. There is a 1–2 μm region of the seal below the patch where proteins are excluded and this may consist of extracted lipids that form the gigaseal. Patch domes often have complex geometries with inhomogeneous stresses due to the membrane-glass adhesion energy (E_a), cytoskeletal forces, and possible lipid subdomains. The resting tension in the patch dome ranges from 1–4 mN/m, a significant fraction of the lytic tension of a bilayer (~10 mN/m). Thus, all patch experiments are conducted under substantial, and uneven, resting tension that may alter the kinetics of many channels. E_a seems dominated by van der Waals attraction overlaid with a normally repulsive Coulombic force. High ionic strength pipette saline increased E_a and, surprisingly, increased cytoskeletal rigidity in cell-attached patches. Low pH pipette saline also increased E_a and reduced the seal selectivity for cations, presumably by neutralizing the membrane surface charge. The seal is a negatively charged, cation selective, space with a resistance of ~7 gigohm/μm in 100 mM KCl, and the high resistivity of the space may result from the presence of high viscosity glycoproteins. Patches creep up the pipette over time with voltage independent and voltage dependent components. Voltage-independent creep is expected from the capillary attraction of E_a and the flow of fresh lipids from the cell. Voltage-dependent creep seems to arise from electroosmosis in the seal. Neutralization of negative charges on the seal membrane with low pH decreased the creep rate and reversed the direction of creep at positive pipette potentials.

INTRODUCTION

The unexpected appearance of a gigohm (GΩ) seal between the cell membrane and a patch pipette ushered in the field of patch clamp electrophysiology (1). The tight seal reduced current noise (1,2) enabling the clear observation of single channel activity (3). However, the original cartoon of patch anatomy as an omega shaped bleb of lipid bilayer in the pipette (4–8) has proven to be oversimplified. The complexity is derived from microdomains of nonuniform stress and composition. When we talk about membrane stress, where does the membrane start and stop? It actually does not have a defined edge but forms a continuum with the cytoskeleton and the extracellular matrix. To avoid confusion with common, but nonspecific terminology, we made a cartoon of a patch (Fig. 1) to define the structural features. To what extent is the patch representative of the in vivo or in situ membrane? Our results show that specific proteins can be excluded or included from patches and that in general the patch dome is of a different composition than the membrane from which it was made.

Guharay and Sachs in 1984 first showed that stretching a patch with suction caused activation of ion channels that proved to be sensitive to membrane tension (9). These are now termed mechanosensitive channels (MSC) or stretch-activated channels and since that time phenotypically similar behavior has been recorded from every phylogenetic kingdom (10). The mechanical sensitivity of channels is not an artifact of patch formation because mechanosensitive currents have been recorded in intact cells (11,12). Mechanical stress modulates many channels that have been characterized previously as voltage-gated including Kv, Ca, and HCN (13–16) or ligand gated (17). Other membrane bound enzymes such as GTPase (18) and phospholipase (19) are also mechanosensitive. Mechanosensitivity arises from dimensional changes between protein conformational states, but these changes are also coupled to reorganization of the surrounding lipids and probably cytoskeleton so that the system under study consists of more than just the protein.

For artificial lipid bilayers the adhesive energy that holds the membrane to the glass is ~1–5 J/m^2 (mN/m) (20), a tension comparable to the lytic limit of a bilayer (~10 mN/m) (21). Patches formed from biological samples differ from bilayers in two distinct features. First, the patch dome is supported by the cortical cytoskeleton (22) that forms a mesh underlying the bilayer (23). Second, biological membranes contain proteins and glycosylation groups that can affect adhesion energy (E_a). Stress in the resting membrane is dominated by E_a and cytoskeletal forces that act both normal and tangential to the plane of the membrane (24). Unstressed patches do not exist, except transiently at the end of a pressure step when the stretched patch is pushed back toward a disk and wrinkles (25).

Gigaseals can form between glass and lipid bilayers (20), or rubber and glass (1,26). But how can an uneven biological membrane with protruding proteins and glycocalyx form

Submitted March 7, 2009, and accepted for publication May 4, 2009.

*Correspondence: suchyna@buffalo.edu

Editor: Richard W. Aldrich.

0006-3495/09/08/0738/10 $2.00

doi: 10.1016/j.bpj.2009.05.018

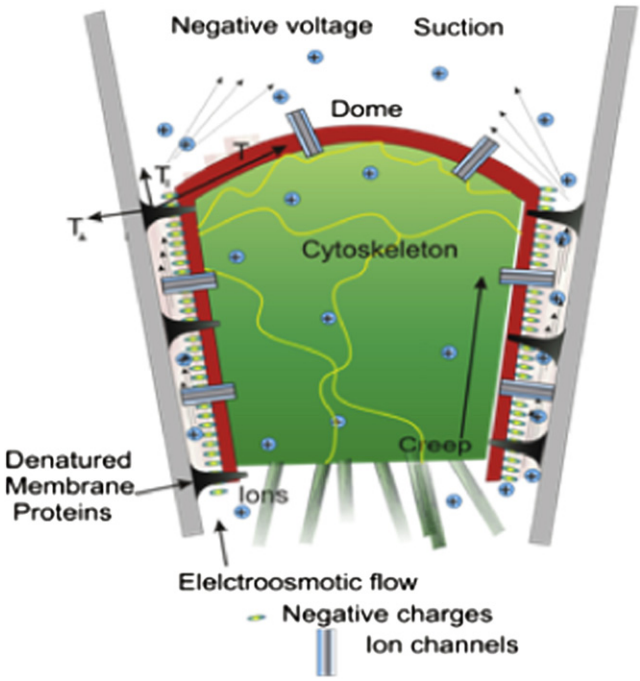

FIGURE 1 Cartoon of patch structure. The patch has three distinct regions: the dome (the characteristic patch of membrane that spans the pipette), the gigaseal between the membrane and the glass that we will approximate as a cylindrical annulus containing saline and extracellular matrix, and the cytoskeleton that forms a porous matrix behind the dome (5,6). We illustrate a patch consisting of a shell of cell cortex (*red*) containing the bilayer that surrounds a plug of cytoplasm (*green*). The space between the bilayer and the glass is called the gigaseal (*yellow* and *white*). It contains fixed charges (nominally negative) attached to both the membrane and the glass. Proteins sticking far from the bilayer are denatured against the glass (*black*). Ion channels (*blue*) that may be mobile and functional are distributed in varying density throughout the dome and the seal.

a tight seal with the glass? We know that some membrane proteins like acetylcholine receptors (AChRs) protrude >5 nm above the bilayer (27), so that the local phospholipids are prevented from reaching the glass. However, structures like AchRs denature against the glass (5) and can pull the adjacent membrane closer to the glass causing the seal to progress like a zipper, which we refer to as a ''fried egg'' model.

The elaborate structure of biological patches is formed by five major forces: 1), membrane tension produced by hydrostatic pressure in the pipette; 2), the normal and tangential stresses from the cytoskeleton that can pull or push on seal and the dome; the cytoskeleton may also act as a porous plug in the tip obstructing water flow so that the trans-patch pressure is less than the applied pressure; 3), electroosmotic drag forces acting in the gigaseal causing a voltage dependent creep (28); 4), the viscosity of the liquid components of the membrane; and 5), the adhesion energy of the membrane to the glass. The method to measure the adhesion energy of the patch was developed by Opsahl and Webb (20), although the basics are known to anyone who has from peeled tape; when tape begins to peel, the normal component of the tension is equal to the adhesion energy.

MATERIALS AND METHODS

See Materials and Methods in the Supporting Material.

RESULTS

Seal formation and patch subdomains

Patch formation occurs by membrane blebbing into the pipette before the gigaseal forms (see Movie S1 in the Supporting Material). Immediately after seal formation, patches assume a variety of irregular shapes such as angled domes, long extensions of folded membrane (Fig. 2 *A*, *panel 1*), and thin filopodia-like extensions (Fig. 2 *B*, *panel 1*) that are likely the result of cytoskeletal forces. These mechanical subdomains mark regions of variable stress, and channels within these domains are unlikely to feel the mean stress when suction is applied to the pipette. Exercising a patch 10–20 times with mild pulses of suction (×30 mm Hg for 500 ms) can disrupt some of the subdomains and yield a dome with uniform curvature (Fig. 2, *A* and *B*, *panel 2*, and Movie S2).

When a channel is in the dome (Fig. 2 *C*, *Dome*), the access resistance is low and the membrane appears electrically as a parallel RC network. The effective patch capacitance is only weakly affected by channel openings, and the patch conductance parallels the channel current. However, a channel that moves from the dome into the seal experiences a different environment (Fig. 2 *C*, *Seal*). Repositioning can occur by diffusion of the channel into the seal or by the seal advancing over the channel as in Fig. 2, *A* and *B*. Once the channel enters the seal, the access resistance becomes comparable to the channel resistance, and the equivalent circuit of the patch has three or more elements. There is now increased coupling between the in-phase (conductance) and quadrature (capacitance) signals. A channel in the seal has a slower rise time, smaller amplitude, and greater open channel noise due to fluctuations in the access impedance.

Irregular patch structures occur most frequently with rapidly remodeling cell types such as CHO, COS7, and HEK (see Movie S3). Myotubes that remodel slowly typically form stable disk shaped domes. The curvature of resting patches represent cytoskeletal interactions because treatment with actin reagents (29) and/or exercising the patches to disrupt the cytoskeleton lead to flat domes (Fig. 2 *A*, *panel 2*), the expected shape of membranes with a small bending moment. However, sometimes patches are concave, pulled toward the tip by actin (8), or remain convex upward pushed by the cytoskeleton (Fig. 2 *B*, *panel 4*). The response of patches to steps of suction differs for these different types of patches, with flat patches showing

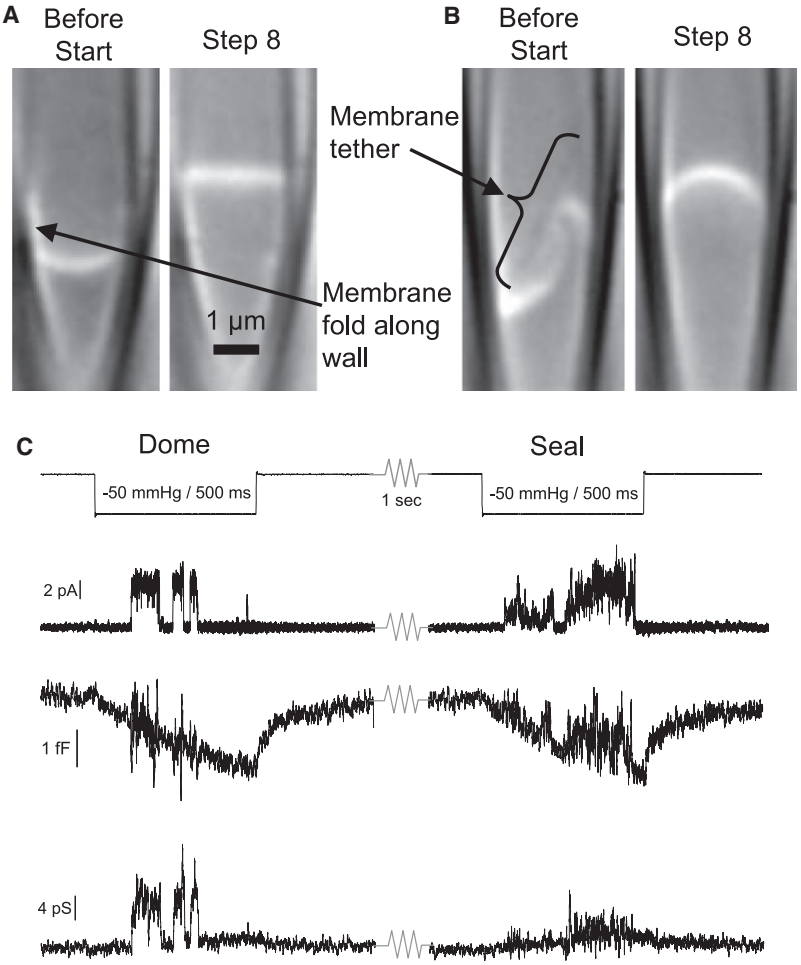

FIGURE 2 DIC microscopy images of patches showing irregular resting patch geometries and restructuring after suction steps (500 ms, −30 mm Hg, 2 s apart). (*A*) An astrocyte patch initially showing a membrane fold adhering to the glass above the dome. That folded membrane expanded producing a higher dome position and the membrane initially exposed to the pipette saline is now part of the seal (see Movie S2). (*B*) COS7 patch showing a membrane tether (*bracket*) and folds. The tether inflates into a bleb and forms part of the dome surface when suction is applied (see Movie S2). (*C*) Channel properties change when the channel moves from the dome to the seal. This example shows MSC channel currents and patch capacitance and conductance for two sequential suction steps (2 s apart, −100 mV). The open state properties change significantly from the first to the second step, and the capacitance and conductance show significant crosstalk during the second stimulus because of the increase in access impedance in the seal.

a more elastic response (see Movie S2). The dome and seal membrane are readily visible in bright field microscopy (Fig. 2) emphasizing that the mechanical membrane is not simply a lipid bilayer but a complex structure (23).

Seal composition and structure

Is the dome membrane identical to the surrounding cell membrane, or does close contact with glass attract some components and exclude others? Because the pipette initially contacts the glycocalyx, we examined the structure of patches made from cells labeled with fluorescently tagged wheat germ agglutinin (WGA). In vitro the cells were asymmetric with adherent surfaces exhibiting bright puncta whereas the upper surface was dimmer and more diffuse (Fig. S4*A*). This heterogeneity emphasizes that a patch formed from the upper surface cannot represent the mean properties of the whole cell. Patches from rat astrocytes showed that the glycocalyx was excluded from all regions of the patch (Fig. S4*B*). However, WGA accumulated at the entrance to the pipette as though it were filtered out by the tip (Fig. S4*C*). Patches from myotubes showed no detectable WGA fluorescence in the dome or the seal (data not shown).

Electron microscopy of the patch has shown that AChRs are densely clustered in the seal and few receptors make it to the dome (5). To observe the distribution of other membrane proteins, we transfected COS and HEK cells with GFP fusion proteins of TRPC6 (Fig. 3 *A*) and TREK-1 (Fig. 3 *B*). Both proteins were present in the seal and the dome. TREK in the cell was strongly attracted to the glass as shown by the intense fluorescence where the tip touched the cell (Fig. 3 *B*, *left panel*). TRPC6 had a punctate distribution in the seal whereas TREK was more uniform, similar to their respective cell surface distributions. Both proteins appeared uniformly distributed in the dome, but because we viewed it from the edge we were not sensitive to variations. When the patches were stressed with suction, only TREK produced mechanosensitive currents, even with three times greater pressure applied to the TRPC6 patch (Fig. 3, *C* and *D*) suggesting that TRPC6 by itself is not mechanosensitive (30,31). Interestingly, both channels were completely excluded from a region ~2 μm below the dome (denoted with asterisk in Fig. 5). This exclusion zone was observed in multiple patches for both proteins. The zone may represent a region where lipids have been extracted from the membrane and bond to the glass and possibly form the actual gigaseal.

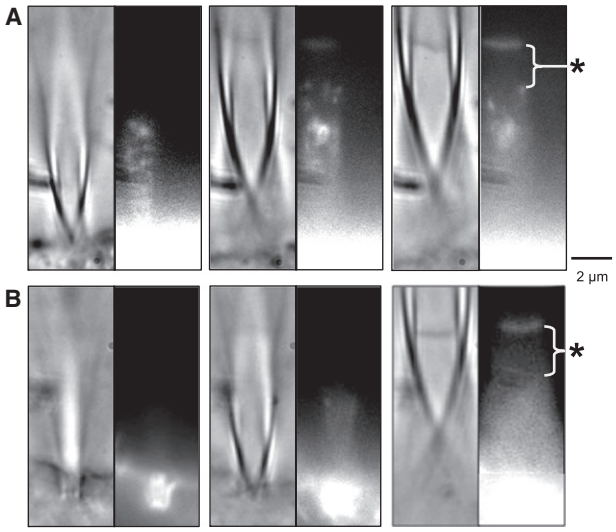

FIGURE 3 A through focus series (1 μm steps) of DIC and fluorescence images showing the distribution of GFP labeled channels within the pipette along with the currents produced when the patches were stretched. The images were taken 1 μm apart with the pipette at ~15° to the coverslip. (*A*) TRPC6-GFP fusion protein expressed in COS cells shows a punctate distribution in the seal that is similar to its distribution on the cell surface but a diffuse distribution in the dome. (*B*) TREK1-GFP fusion protein expressed in HEK cells has a more diffuse distribution on the cell surface than TRPC6, and shows a diffuse surface distribution in the seal and the dome. Both proteins, especially TREK, show aggregation about the tip. There is an exclusion zone of a ~2 μm band beneath the patch dome that is devoid of both TRPC6 and TREK (*). (*C*) Stretching the TRPC6 patch produced no MSC current at $\pm$50 mV pipette potential, but the TREK patches (*D*) produced a robust current that reversed at ~−50 mV as expected for a K^+ selective channel. The patch currents are averages from 5–6 pressure steps.

Adhesion force

The strain of the dome in response to pipette pressure represents an interaction of forces generated from pressure, the cytoskeleton, and the adhesion energy. As expected, suction causes the patch to bulge upward (Fig. 4 *A*), and for a two dimensional structure with no bending moment, E_a can be estimated from the membrane tension and the angle of contact with the glass (20). However, biological patches are mechanically three dimensional due to the cytoskeleton and they respond to a suction step with viscoelastic relaxation (see Fig. 4 *A*, *inset*, and Suchyna and Sachs (8,32)). Needing to keep the suction pulses short to minimize creep, we estimated the steady-state dome height from an exponential fit. We also used only negative pressure because positive pressure causes flow of new membrane into the dome so that we could not achieve steady-state. In cell-attached mode, our estimate of E_a is probably low because the cytoskeleton tends to pull the membrane away from the pipette. We compared E_a in myotubes, astrocytes, and HEK cells to determine if membrane composition had a significant effect. The kinetics of patch strain were different (see Fig. 6 *B*), with myotubes having the slowest response, but the deformation rates correlated qualitatively with the visible remodeling rates of intact cells (see Movie S3). E_a, however, was nearly identical in all cell types ~1.6 mN/m (Fig. 4 *C*), and was independent of the applied pressure (Fig. 4, *D* and *E*), the patch diameter (Fig. 4 *F*), and the pipette potential (data not shown).

The Coulombic contribution to E_a was shown by varying the ionic composition of the saline in the pipette (Fig. 5 *A*, all data from astrocytes). The specific resistance of the seal decreased with increasing ionic strength: ~7 GΩ/μm at 100 mM KCl, ~14 GΩ/μm at 10 mM, and ~3 GΩ/μm at 300 mM suggesting that the ionic content of the seal is continuous with the pipette solution and that it is the upper part of the seal that determines the resistance. Forming seals with high ionic strength in the electrode required strong suction, and many of the resulting patches were highly vesiculated with irregularly shaped domes having no defined radius of curvature (Fig. 5 *B* and Movie S5). The patches that produced spherical dome shapes were stiff, deforming little with suction (Fig. 5 *C*), and exhibiting small capacitance changes (Fig. 5 *D*). The large E_a observed in high salt may be an artifact due to cytoskeletal stiffening or clogging of the pipette tip so that trans-dome pressure is less than the pipette pressure.

To determine if stiffening was due to osmotic water depletion or ionic strength, we made patches with pipettes containing hypertonic solutions of normal salt (100 mM KCl) augmented with 400 mM mannitol. These patches formed more slowly than controls but deformed to a similar extent. At low ionic strength (10 mM KCl), E_a was similar to controls but the patches showed a faster mechanical response suggesting a more compliant cytoskeleton. E_a was unaffected by Ca^{2+} (Fig. 5 *A*) except at 20 mM where there is a substantial increase in ionic strength.

The remarkable stiffening of the cytosol at high (pipette) ionic strength was reflected with high resolution in the record of patch capacitance (Fig. 5 *D*). Tension normally peels the membrane from the seal producing increases in capacitance, but solutions with high osmotic pressures showed a transient decrease in capacitance during a suction step. This decrease in electrical area may occur because the viscous cytoskeletal core initially translates as a block, driving some dome membrane against the glass.

Priel et al. (33) showed that low pH increases membrane adhesion to glass likely through Coulombic forces or H-bonding (note that they used a mechanical, not electrical,

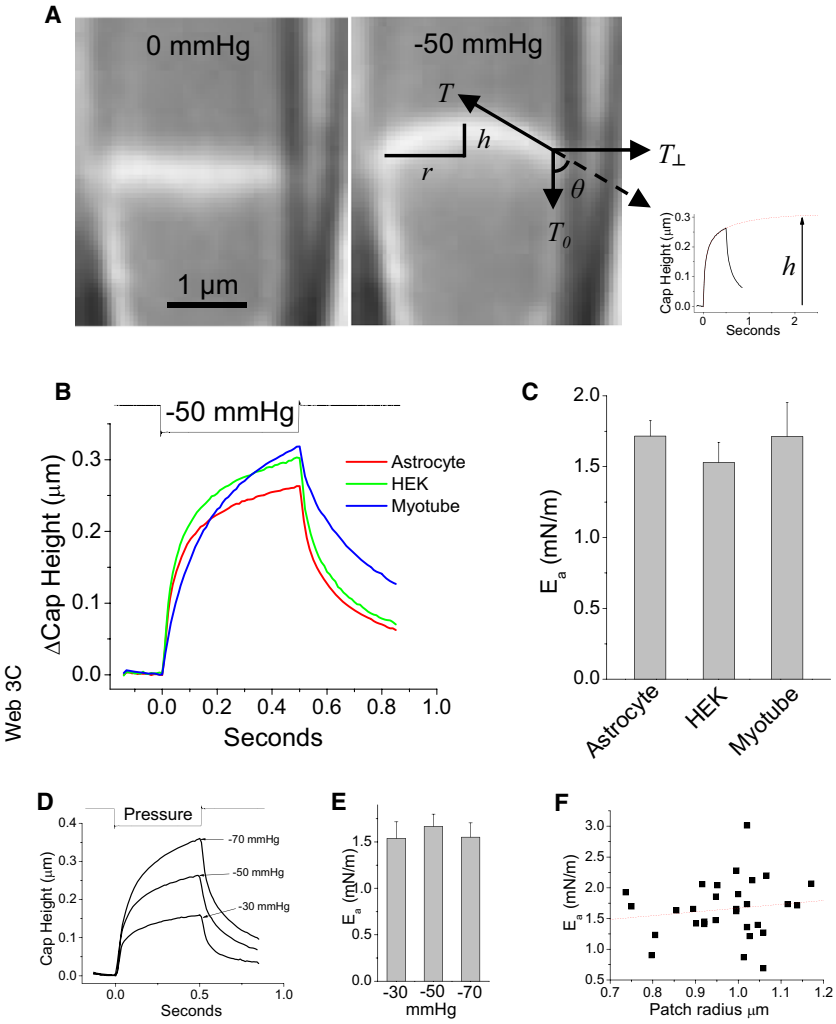

FIGURE 4 (*A*) Calculating E_a. The membrane tension at equilibrium is estimated from Laplace's law $T = R_C \times P/2$, where R_C is the radius of curvature calculated from the patch radius (r) and dome height (h) and P is the pressure gradient. The tension is resolved into two orthogonal components and the adhesion energy is then calculated by: $E_a = T_\perp = T - T \times \cos\theta$. The dome height follows an exponential time course that is extrapolated to extract the equilibrium geometry (*inset*). E_a is independent of membrane composition, stimulus strength and patch radius. (*B*) Shows the average motion of the dome center for cell-attached patches from three cell types; astrocytes, $n = 11$, $r = 0.93 \pm 0.04$ μm; HEK, $n = 7$, $r = 0.97 \pm 0.01$ μm; mouse myotubes, $n = 9$, $r = 1.02 \pm 0.04$ μm. (*C*) E_a differs little between cell types. (*D*) Dome height (strain) versus time for astrocyte patches at different pressures. (*E*) E_a is independent of stimulus pressure within the range normally used to activate MSCs. (*F*) E_a from independent patches shows that E_a is nearly independent of the patch radius.

seal so results may differ). In this study, at high ionic strength the stiff cytoskeleton made it difficult to measure E_a whereas lower ionic strength showed little affect, making it difficult to assess the Coulombic force contribution to E_a. However, similar to Priel et al. (33), we found E_a was dependent on pH increasing threefold at pH 5 and decreasing twofold at pH 9 (Fig. 5, *A* and *E*) while showing similar deformation rates, suggesting weak cytoskeletal effects. Paradoxically, despite a larger E_a at pH 5, seal formation required higher suction (−15 to −30 mm Hg) than at pH 9 where seals formed readily at normal suction. Apparently bleb inflation into the pipette and seal formation are different processes.

Excised patches reduce cytoskeletal contribution

Reduced cytoskeletal interference should give us a better estimate of E_a so we carried out the same analyses on inside-out patches. The loss of cytoplasmic components and possible unfolding of membrane domains was visible as a ~10-fold lower optical density of the dome (Fig. 6 *A*). Inside-out patches relaxed ~5-fold faster than cell-attached showing that the strain kinetics are dominated by the cytoskeleton (Fig. 6 *B*). For excised patches in control saline, E_a doubled to ~3 mN/m (Fig. 6 *C*, pH 7). In cell-attached mode the cytoskeleton may transfer some of the force of dome deformation diagonally to the seal helping to pull the membrane from the glass. Low ionic strength pipette saline decreased the stability of inside-out patches to stimulation. Excision with high ionic strength pipette saline either produced vesicles in the tip or pulled the entire patch out of the pipette. We were able to form inside-out patches at different pipette pH. Similarly to cell-attached patches, E_a for inside-out patches at pH 9 was ~50% that at pH 7. Interestingly, at pH 5, E_a decreased from the cell-attached values. However, many of the pH 5 patches ruptured before suction could be applied possibly biasing the results (see Discussion).

Patch creep—a function of E_a and electroosmosis

Cell-attached patches creep continuously up the pipette at 0.5–1 μm/min even in the absence of suction (8,28,34). This capillary action is caused by E_a and the presence of a liquid membrane, but the motion is also voltage sensitive

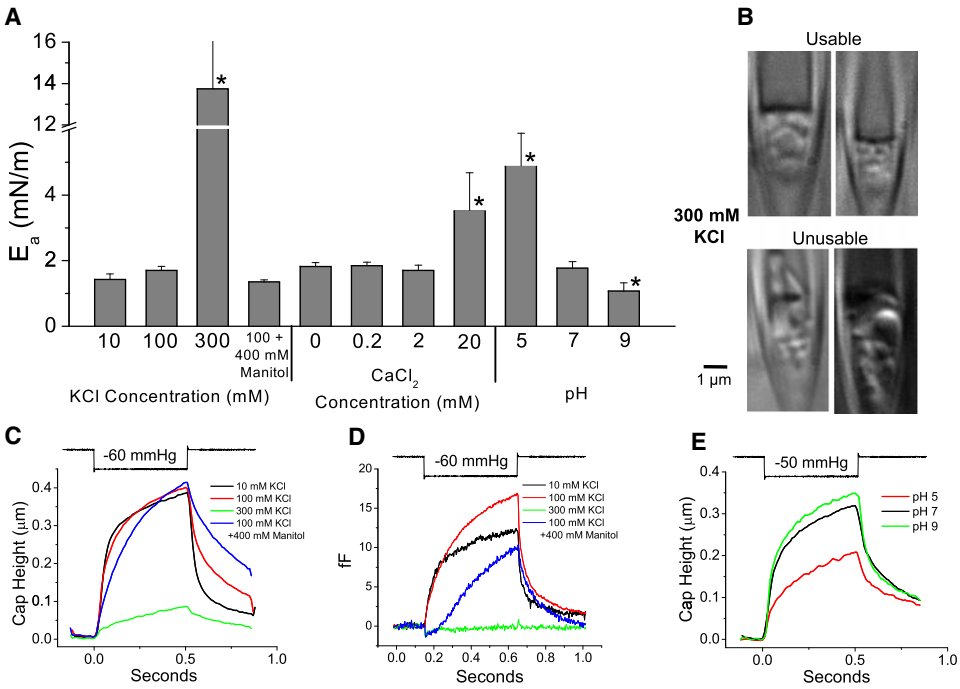

FIGURE 5 Ionic and osmotic strength affect E_a and the structure of cell-attached patches from astrocytes. (*A*) KCl (300 mM) in the pipette produced clumps of cytoskeletal hardened blebs in the patch that often formed irregular dome shapes unusable for analysis. (*B*) The ensemble average dome motion was compared for four different solutions containing 5 mM HEPES × KOH pH 7 with the indicated concentrations of KCl and mannitol. Patches in 300 mM KCl (*green trace*, $n = 10$, $r = 0.92 \pm 0.05$) showed a dramatic decrease in deformability. This effect was not due to high osmotic pressure because patches in 100 mM KCl complemented with 400 mM mannitol (*blue trace*, $n = 5$, $r = 1.05 \pm 0.02$) were similar to controls (100 mM KCl, *red trace*, $n = 8$, $r = 1.08 \pm 0.05$). Lowering the ionic strength to 10 mM KCl (*black trace*, $n = 7$, $r = 0.98 \pm 0.12$) produced faster kinetics. (*C*) Strain kinetics revealed in high resolution by patch capacitance. Note that patches in high osmotic pressure pipette solutions displayed a transient drop in capacitance after a step of suction, and there was no significant increase in capacitance in 300 mM KCl suggestive of a stiff patch. (*D*) Acidic pH in the pipette significantly decreased patch deformability, whereas alkaline pH had the opposite effect (pH 5, $n = 10$, $r = 1.25 \pm 0.04$; pH 7, $n = 8$, $r = 1.03 \pm 0.05$; pH 9, $n = 5$, $r = 0.88 \pm 0.05$) although the strain kinetics were unchanged. Pipette saline contained 100 mM KCl and 5 mM HEPES at the pH shown. At pH 9 patches formed much closer to the tip so that the average patch diameter was ~15% smaller than at pH 7. (*E*) E_a for different ionic, osmotic strength, and pH. The bars with an asterisk are significantly different from controls. High ionic strength increases E_a that may be an artifact of cytoskeletal stiffening. E_a was only weakly sensitive to Ca^{2+} in the pipette (0.2 mM, $n = 8$; 2 mM, $n = 8$), but 20 mM $CaCl_2$ ($n = 6$) produced a significant increase in E_a, mimicking the effect of increasing KCl concentration. Acidic pH increased E_a whereas alkaline pH had the opposite effect (see Fig. 8).

(see Fig. 7 *A* and Gil et al. (34)). Creep in patches from excitable cells like myotubes was more than twice as voltage sensitive as patches from nonexcitable cells like astrocytes. At pH 7, the creep rate was always faster for negative than for positive pipette potentials. High ionic strength in the pipette decreased the creep rate (Fig. 7 *B*) probably due to changes in cytoskeletal stiffness or shielding of fixed surface charges in the seal. The creep rate was not sensitive to osmotic pressure or small changes of Ca^{2+} concentration in the pipette. Acidic pipette pH, which increased E_a, did not significantly affect the creep rate, but basic pH decreased it.

To better understand creep, we examined inside-out patches where cytoskeleton is depleted and the amount of membrane is limited. Because creep involves the entire seal, we used symmetrical bath and pipette solutions. In contrast to cell-attached patches, inside-out patches showed no creep at 0 mV as expected because there was no supply of new membrane. However, inside-outs displayed voltage dependent creep, even changing direction with polarity (Fig. 8 *A*). Creep motion is established within seconds of the voltage change. The direction and rate of voltage-dependent creep was pH dependent. At pH 7 the patches move upward for negative potentials and downward for positive. The direction of motion was the same at pH 7 and 9, but the velocity was higher for pH 9. However, at pH 5 the direction reversed polarity. This suggests that titratable surface charges in the seal dominate voltage dependent creep. At pH 7 the magnitude of creep rate for positive and negative voltages was about the same, but in opposite directions. The voltage sensitivity decreased at acidic pH and increased at alkaline pH (Fig. 8 *B*). The electromotive force that moves the patch seems to be electroosmosis, the coupling of ion flow to water flow. This was supported by using patches formed in soft glass with lower surface charge (Fig. S6) showing reduced voltage dependent creep (Fig. S7). With negative charges on both the membrane and the glass the space is cation selective and voltage applied across the seal (from pipette to bath) will generate a flow of mobile cations. These ions will drag water in the space and hence the membrane. The cation selectivity of the seal space was shown previously in seals formed between Sylgard (Dow Corning, Midland, MI) and glass (26). We predicted that replacing the more mobile cation (K^+) with the larger, less mobile, cation ($NMDG^+$) would slow the voltage induced creep, and this produced a 10-fold reduction in creep rate without affecting the direction (Fig. 8 *B*).

If the voltage dependence of creep is due to electroosmosis, we expected that applying suction to the patch should produce streaming potentials from the seal as seen in the glass-Sylgard seals (26). We did observe potential changes with negative pressure steps, but the potentials were unstable possibly because changes the seal resistance and the

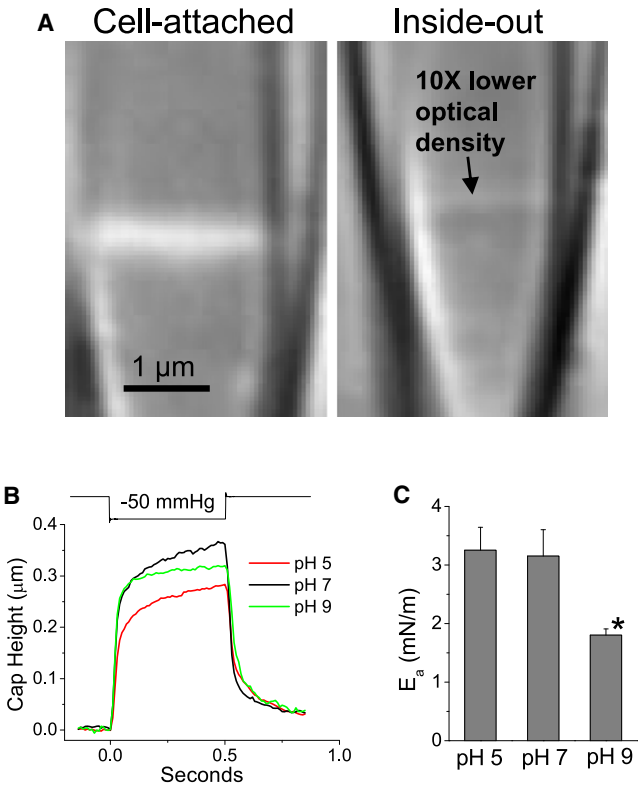

FIGURE 6 Inside-out patches from astrocytes have less cytoskeleton and respond differently to suction than cell-attached. (*A*) Optical density of excised patches is 10-fold lower than cell attached patches, illustrating the loss of cytoplasm. (*B*) Average patch motion from inside-out patches with the pipette saline at different pH shows faster kinetics than cell-attached. (*C*) E_a for pH 7 ($n = 4$, $r = 1.25 \pm 0.15$ μm) and pH 5 ($n = 4$, $r = 1.19 \pm 0.07$ μm) were significantly greater than in cell-attached mode. At pH 9 ($n = 3$, $r = 0.94 \pm 0.05$ μm) patches showed significantly lower E_a than pH 7, but still greater than in cell-attached mode.

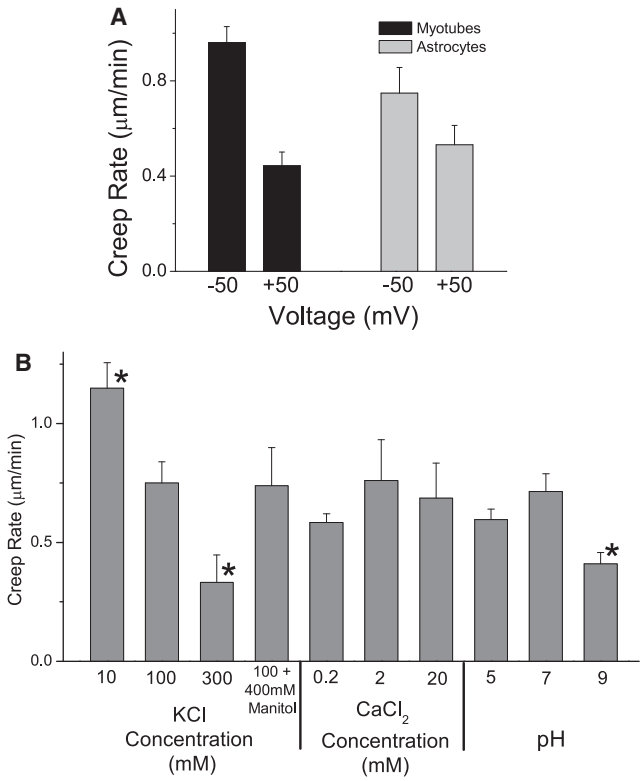

FIGURE 7 Cell-attached patches creep up the inside of the pipette at 0 mm Hg. The creep rate of the edge of the dome was measured during relaxation between suction steps. (*A*) Astrocytes ($n = 11$) and myotubes ($n = 9$) both show increased creep rate at negative pipette voltages. Pipette voltage is shown instead of membrane voltage because the relevant potential difference along the seal is between the pipette and the bath. (*B*) The creep rate measured at 0 mV slowed with increasing ionic strength, being almost four times faster in 10 mM than in 300 mM KCl. Osmotic strength and divalent concentration had no effect on creep rate, but pH 9 slowed creep to about half the normal rate whereas pH 5 had little effect.

amplifier's bias current changes the voltage (see Fig. S6 for a discussion of streaming potential theory).

DISCUSSION

Membrane blebbing precedes seal formation and affects patch structure

We observed that most patches form by a process of bleb inflation into the pipette (typically multiple times) before forming a seal. Blebs rarely form in normal cells where the internal resting pressure is ~+100 Pa (0.13 ATM) (35), but commonly form on cells where membrane-cytoskeleton adhesion is reduced. Blebbing in the pipette is induced by suction (2–4 mm Hg or ~250–500 Pa). Blebs form on cells by delamination (tearing the membrane from the cortex) and lipid flow into the bleb (as when pulling a tether). This results in phase separations where the newly blebbed membrane has significantly different composition than the average cell surface (36). Depletion of cytoskeleton in a bleb increases mobility of the remaining components (37) and likely accounts for the observed redistribution and/or exclusion of glycosylation groups (Fig. S4) and GFP-tagged channels (Fig. 3). The "exclusion zone" immediately beneath the dome is an extreme case of redistribution (see the new patch model in Fig. S8). If the zone is made of lipids extracted from the membrane and bound to the glass, this could be the actual gigaseal. If so, this may explain how membranes with protruding proteins form seals.

Mechanical microdomains within the patch

Just as blebs formed in vivo are retracted after 1–2 min (35), the cortex reforms beneath the dome within seconds to minutes after seal formation. The cytoskeleton adapts to the new stresses from E_a and the physical constraints of the tip forming microdomains like those shown in Fig. 2, and other optically invisible structures. Stress gradients broaden the dose-response characteristics of mechanosensitive channels (16). The presence of mechanical domains is not an artifact of the patch clamp because mechanical domain transitions can also be seen in whole cell recordings

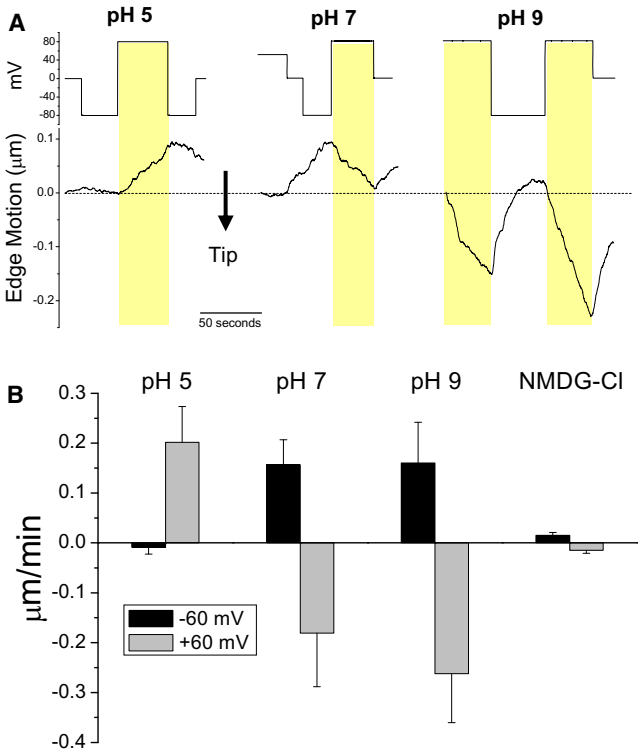

FIGURE 8 (*A*) Edge motion from inside-out patches at 0 mm Hg was voltage and pH dependent, but small compared to cell-attached patches. The differences in creep rate at +80 mV pipette potential are shaded for comparison. Voltage sensitive creep rate is pH sensitive with pH 5 patches moving upward at +80 mV pipette potential, slowly downward at pH 7, and rapidly downward at pH 9. The reverse effect was observed at −80 mV. (*B*) Average motion from 3–4 inside-out patches at different pH with ±60 mV pipette potential. Note that both the direction and the rate of patch motion change. The rate differences were 2.1, 3.4, and 4.3 μm/min for pH 5, 7, and 9, respectively. Average edge motion for patches at pH 7 exposed to symmetrical 140 mM NMDG-Cl decreased creep ~10-fold supporting the idea that the seal is cation selective and the creep rate depends on ion drift velocity.

(11). The domains can be partially disrupted by mechanically ''exercising'' the patch (Fig. 2). Because most patch clamp studies do not include an exercise protocol, substantial stress gradients are likely to exist, and relaxation of these gradients could produce responses classified as rundown or run up. However, even flat patches have high tension compared to the cell so there are practical limits to simplifying the patch.

Adhesion energy

The primary attractive force for the gigaseal seems to be van der Waals attraction, the same forces that account for the tape adhesion (38). Van der Waals interactions are not a chemically specific force and apply to glass, proteins, polysaccharides, and lipids. In the seal this attraction appears overlaid with electrostatic repulsion. In cell-attached patches, E_a was consistent at ~1.6 mN/m regardless of cell type, stimulus magnitude, patch dimensions, and pipette voltage. Increased ionic strength or decreased pH in the pipette affected E_a but in cell-attached patches this sensitivity was due partly to modified cytoskeletal properties. The transmembrane coupling of high ionic strength pipette saline to the cytoskeleton seems similar to phenomena in whole cells where hypertonicity induces recruitment of ezrin/radixin/moesin proteins to the membrane causing stiffening (see Rasmussen et al. (39) and Discussion in Movie S5). However, at low pH, neither the patch (Fig. 7) nor the whole cells (39) exhibited cytoskeleton stiffening. The reduced deformation of patches in low pH is more likely the result of increased E_a due to the positive charges on the membrane attracting the negative glass.

Inside-out patches more closely approximate a planar bilayer due to depletion of the cytoskeleton. Thus the E_a of inside-out patches, ~3.2 mN/m, is likely to be a better estimate of the adhesion energy than the cell-attached estimate. In general, inside-out patches were more susceptible to breakage by suction than cell-attached patches. However, at pH 5 inside-out patches were more unstable than at pH 7 or pH 9 and would often rupture before they could be tested. Decreased cytoskeletal reinforcement of inside-out patch reduces the lytic strength closer to the resting tension of 3–4 mN/m. This may lead to an unintended bias in patch recordings where the user selects ''surviving'' patches, i.e., those with less disrupted cytoskeleton.

Patch creep

The cell provides an effectively infinite supply of lipids where adhesion of membrane to glass causes cell-attached patches to creep continuously up the pipette at ~1 μm/min. Inside-out patches, that have a fixed amount of membrane don't creep, but they can be driven by the pipette potential at a rate that is sensitive to both ionic strength and pH. Voltage-dependent creep seems to be the result of electroosmotic flow through the seal. As mobile ions migrate through the seal (the leakage current) they drag water that in turn drags the adjacent membrane. The seal space is normally negatively charged by both the glass and the membrane making the space cation selective and accounts for: a), the reversed voltage dependent creep at low pH where protons titrate the negative charge in the seal creating an anion conducting space; and b), creep is 10 times faster with K^+ than $NMDG^+$. However in the latter case, K^+ has only three times greater aqueous mobility of $NMDG^+$ suggesting the seal space is more complicated than simple saline.

Electroosmotic forces are proportional to surface charge density and are symmetric in the voltage field (see Electroosmosis and Creep in the Supporting Material for a more detailed explanation of this force). This explains why the creep rate is sensitive to factors that affect surface charge such as the ionic strength, pH, and glass and membrane composition. However, we did observe some unpredicted asymmetries in the voltage dependence (low pH (Fig. 8) and soft glass (Fig. S7)) that may be the result of electrophoresis of the patch itself or asymmetries in the seal.

Resistance of the seal

The specific resistance of seals in 100 mM KCl was $R_s \sim 7$ GΩ/μm assuming that the length of the seal is from the edge of the dome to the tip of the pipette. A pipette of 1 μm radius with a 10-μm long seal filled with 100 mM KCl (0.85 Ω-m) would have a seal resistance of only $R = 0.14/h$, or 1.4 GΩ for $h = 1$ nm, and 0.3 GΩ for $h = 5$ nm, a space thick enough to accommodate an intact AchR. So how can we get seal resistances in the range of 10–200 GΩ from an irregular surface? One possibility is the exclusion zone where only lipids contact the glass (Fig. S8). Alternatively, the viscosity of the space could be much higher than water. If the space had ~50× the viscosity of water, similar to 80% glycerol or 60% sucrose, the seal resistance would be in the observed range. If we imagine the extracellular proteins and glycocalyx (40) compressed into the seal like caulking, high viscosity seems a reasonable explanation.

What happens to channels in the labile environment of a patch? They may diffuse from the seal to the dome or vice versa as shown in Fig. 2, and this ''partial seal'' behavior emphasizes that the seal is not discrete but distributed (32). Channels in the partial seal can contribute current to the recording, but will have modified properties due to the cable properties of the seal access impedance. Channel openings in the seal will have a slower rise time and lower current amplitude, similar to what was reported for glutamate channels in locust muscle (41). Channels active in the seal will generate a water flow that may modulate the seal thickness and produce fluctuations in accesses impedance. This modulation may account for low frequency open channel noise.

Is the patch representative of the cell membrane?

The formation of a patch leads to a redistribution of components that can be sustained over the lifetime of a patch. This could create differences between whole-cell and patch data. For example, using a variety of stimuli, Hamill et al. (42) were unable to activate whole-cell cation selective MSCs currents in oocytes whereas those currents were common in patches. Others have observed that patch currents can be comparable to whole cell currents for TREK (P. Gottlieb and F. Sachs, unpublished data) and TRPV1 (Feng Qin, State University of New York at Buffalo, personal communication, 2008). If all the channels that were in the exclusion zone beneath the patch moved to the dome during seal formation, then the density in the dome would be ~5 times greater than the cell, not enough to account for the discrepancy in amplitudes. Channels may also be concentrated by attraction to the glass (Fig. 3 *B*, *left pair*).

Changes in membrane composition that accompany patch formation lead to new mechanical domains. Domains in the patch can be lipid-lipid phases (43) or cytoskeletal in origin but they both contribute via line tension (44) to the interior stress tending to isolate interior channels. Despite significant rearrangements associated with patch formation, after ''exercising'' the patch and allowing it to relax, the mechanical properties retain some of the distinctive properties of the cell type from which it was formed. Patches that are made from slowly remodeling cells like myotubes produce patches that respond more slowly than patches from rapidly remodeling cells like HEK and CHO. Similarly, patches from normal and dystrophic muscle cells reflect the differences in cortical properties produced by the loss of dystrophin (8). A combination of increased cortical viscosity (8) and reduced strength of association with the deeper cytoskeleton (45) can provide clues to contractile dysfunction in dystrophic muscle (46).

The patch is a sample of the cell cortex rather than a bilayer, and although this more exacting image of patch structure may complicate the interpretation of electrophysiological data obtained from a patch, that complexity is also the basis for a unique preparation in which to study cortical mechanics and channel activity. MSCs that respond to local stress are a unique probe of membrane mechanics, and it is possible that the physiological function of MSCs in nonspecialized cells are as sensors that detect weakness of the local cytoskeleton (47).

SUPPORTING MATERIAL

Methods, movies, figures, additional text, and references are available at http://www.biophysj.org/biophysj/supplemental/S0006-3495(09)01021-2.

This work was funded by the National Institutes of Health (grant R01 HL054887 to F.S.).

REFERENCES

1. Hamill, O. P., A. Marty, E. Neher, B. Sakmann, and F. J. Sigworth. 1981. Improved patch-clamp techniques for high-resolution current recording from cells and cell-free membrane patches. *Pflugers Arch.* 391:85–100.
2. Colquhoun, D., and F. J. Sigworth. 1983. Single-Channel Recording. Plenum Press, New York, New York.
3. Sakmann, B., and E. Neher. 1983. Geometric parameters of pipettes and membrane patches. *In* Single-Channel Recording. Plenum Press, New York, New York. 37–51.
4. Sokabe, M., F. Sachs, and Z. Jing. 1991. Quantitative video microscopy of patch clamped membranes—stress, strain, capacitance and stretch channel activation. *Biophys. J.* 59:722–728.
5. Ruknudin, A., M. Song, A. Auerbach, and F. Sachs. 1989. The structure of patch clamped membranes in high voltage electron microscopy. *Proc. Elec. Mic. Soc. Am.* 47:936–937.
6. McEwen, B. F., M. J. Song, A. Ruknudin, D. P. Barnard, J. Frank, et al. 1990. Tomographic three dimensional reconstruction of patch clamped membranes imaged with the high voltage electron microscope. *XII International Conference of Electron Microscopy*. Baltimore, MD. 522–523.
7. Milton, R. L., and J. H. Caldwell. 1990. How do patch clamp seals form? *Pflugers Arch.* 416:758–765.
8. Suchyna, T. M., and F. Sachs. 2007. Mechanosensitive channel properties and membrane mechanics in mouse dystrophic myotubes. *J. Physiol.* 581:369–387.
9. Guharay, F., and F. Sachs. 1984. Stretch-activated single ion channel currents in tissue-cultured embryonic chick skeletal muscle. *J. Physiol.* 352:685–701.

10. Hamill, O. P., and B. Martinac. 2001. Molecular basis of mechanotransduction in living cells. *Physiol. Rev.* 81:685–740.

11. Bett, G. C. L., and F. Sachs. 2000. Whole-cell mechanosensitive currents in rat ventricular myocytes activated by direct stimulation. *J. Membr. Biol.* 173:255–263.

12. Isenberg, G., V. Kazanski, D. Kondratev, M. F. Gallitelli, I. Kiseleva, et al. 2003. Differential effects of stretch and compression on membrane currents and [Na+](c) in ventricular myocytes. *Prog. Biophys. Mol. Biol.* 82:43–56.

13. Morris, C. E., and P. F. Juranka. 2007. Nav channel mechanosensitivity: activation and inactivation accelerate reversibly with stretch. *Biophys. J.* 93:822–833.

14. Calabrese, B., I. V. Tabarean, P. Juranka, and C. E. Morris. 2002. Mechanosensitivity of N-type calcium channel currents. *Biophys. J.* 83:2560–2574.

15. Gu, C. X., P. F. Juranka, and C. E. Morris. 2001. Stretch-activation and stretch-inactivation of *Shaker*-IR, a voltage- gated K^+ channel. *Biophys. J.* 80:2678–2693.

16. Schmidt, D., and R. MacKinnon. 2008. Voltage-dependent K^+ channel gating and voltage sensor toxin sensitivity depend on the mechanical state of the lipid membrane. *Proc. Natl. Acad. Sci. USA.* 105:19276–19281.

17. Paoletti, P., and P. Ascher. 1994. Mechanosensitivity of NMDA receptors in cultured mouse central neurons. *Neuron.* 13:645–655.

18. Gudi, S., J. P. Nolan, and J. A. Frangos. 1998. Modulation of GTPase activity of G proteins by fluid shear stress and phospholipid composition. *Proc. Natl. Acad. Sci. USA.* 95:2515–2519.

19. Lehtonen, J. Y., and P. K. Kinnunen. 1995. Phospholipase A2 as a mechanosensor. *Biophys. J.* 68:1888–1894.

20. Opsahl, L. R., and W. W. Webb. 1994. Lipid-glass adhesion in giga-sealed patch-clamped membranes. *Biophys. J.* 66:75–79.

21. Kwok, R., and E. Evans. 1981. Thermoelasticity of large lecithin bilayer vesicles. *Biophys. J.* 35:637–652.

22. Akinlaja, J., and F. Sachs. 1998. The breakdown of cell membranes by electrical and mechanical stress. *Biophys. J.* 75:247–254.

23. Morone, N., C. Nakada, Y. Umemura, J. Usukura, and A. Kusumi. 2008. Three-dimensional molecular architecture of the plasma-membrane-associated cytoskeleton as reconstructed by freeze-etch electron tomography. *Methods Cell Biol.* 88:207–236.

24. Bowman, C. L., P. A. Gottlieb, T. M. Suchyna, Y. K. Murphy, and F. Sachs. 2007. Mechanosensitive ion channels and the peptide inhibitor GsMTx-4: history, properties, mechanisms and pharmacology. *Toxicon.* 49:249–270.

25. Honore, E., T. Suchyna, A. A. Patel, and F. Sachs. 2006. Desensitization of cloned 2P domain K channels. *Proc. Natl. Acad. Sci. USA.* 103:6859–6864.

26. Sachs, F., and Q. Feng. 1993. Gated, ion selective channels observed with patch pipettes in the absence of membranes: novel properties of the gigaseal. *Biophys. J.* 65:1101–1107.

27. Unwin, N. 1995. Acetylcholine receptor channel imaged in the open state. *Nature.* 373:37–44.

28. Gil, Z., K. L. Magleby, and S. D. Silberberg. 1999. Membrane-pipette interactions underlie delayed voltage activation of mechanosensitive channels in *Xenopus* oocytes. *Biophys. J.* 76:3118–3127.

29. Sokabe, M., and F. Sachs. 1990. The structure and dynamics of patch-clamped membranes: a study by differential interference microscopy. *J. Cell Biol.* 111:599–606.

30. Spassova, M. A., T. Hewavitharana, W. Xu, J. Soboloff, and D. L. Gill. 2006. A common mechanism underlies stretch activation and receptor activation of TRPC6 channels. *Proc. Natl. Acad. Sci. USA.* 103:16586–16591.

31. Voets, T., and B. Nilius. 2009. TRPCs, GPCRs and the Bayliss effect. *EMBO J.* 28:4–5.

32. Suchyna, T., and F. Sachs. 2004. Dynamic regulation of mechanosensitive channels; capacitance used to monitor patch tension in real time. *Phys. Biol.* 1:1–18.

33. Priel, A., Z. Gil, V. T. Moy, K. L. Magleby, and S. D. Silberberg. 2007. Ionic requirements for membrane-glass adhesion and giga seal formation in patch-clamp recording. *Biophys. J.* 92:3893–3900.

34. Gil, Z., S. D. Silberberg, and K. L. Magleby. 1999. Voltage-induced membrane displacement in patch pipettes activates mechanosensitive channels. *Proc. Natl. Acad. Sci. USA.* 96:14594–14599.

35. Charras, G. T. 2008. A short history of blebbing. *J. Microsc.* 231:466–478.

36. Charras, G. T., M. Coughlin, T. J. Mitchison, and L. Mahadevan. 2008. Life and times of a cellular bleb. *Biophys. J.* 94:1836–1853.

37. Sheetz, M. P., J. E. Sable, and H. G. Dobereiner. 2006. Continuous membrane-cytoskeleton adhesion requires continuous accommodation to lipid and cytoskeleton dynamics. *Annu. Rev. Biophys. Biomol. Struct.* 35:417–434.

38. Parsegian, A. 2006. Van der Waals Forces: A Handbook for Biologists, Engineers and Physicists. Cambridge University Press, New York.

39. Rasmussen, M., R. T. Alexander, B. V. Darborg, N. Mobjerg, E. K. Hoffmann, et al. 2008. Osmotic cell shrinkage activates ezrin/radixin/moesin (ERM) proteins: activation mechanisms and physiological implications. *Am. J. Physiol. Cell Physiol.* 294:C197–C212.

40. Weinbaum, S., J. M. Tarbell, and E. R. Damiano. 2007. The structure and function of the endothelial glycocalyx layer. *Annu. Rev. Biomed. Eng.* 9:121–167.

41. Dudel, J., C. Franke, H. Hatt, R. L. Ramsey, and P. N. Usherwood. 1988. Rapid activation and desensitization by glutamate of excitatory, cation-selective channels in locust muscle. *Neurosci. Lett.* 88:33–38.

42. Zhang, Y., and O. P. Hamill. 2000. On the discrepancy between whole-cell and membrane patch mechanosensitivity in *Xenopus* oocytes. *J. Physiol.* 523:101–115.

43. Rawicz, W., B. A. Smith, T. J. McIntosh, S. A. Simon, and E. Evans. 2008. Elasticity, strength, and water permeability of bilayers that contain raft microdomain-forming lipids. *Biophys. J.* 94:4725–4736.

44. Markin, V. S., and F. Sachs. 2004. Thermodynamics of mechanosensitivity. *Phys. Biol.* 1:110–124.

45. Rybakova, I. N., J. R. Patel, and J. M. Ervasti. 2000. The dystrophin complex forms a mechanically strong link between the sarcolemma and costameric actin. *J. Cell Biol.* 150:1209–1214.

46. Claflin, D. R., and S. V. Brooks. 2008. Direct observation of failing fibers in muscles of dystrophic mice provides mechanistic insight into muscular dystrophy. *Am. J. Physiol. Cell Physiol.* 294:C651–C658.

47. Charras, G. T., C. K. Hu, M. Coughlin, and T. J. Mitchison. 2006. Reassembly of contractile actin cortex in cell blebs. *J. Cell Biol.* 175:477–490.